Materials Research Bulletin 71 (2015) 67–74

Contents lists available at ScienceDirect

Materials Research Bulletin

journal homepage: www.elsevier.com/locate/matresbu

Dielectric silicone elastomers with mixed ceramic nanoparticles

George Stiubianu[a,*], Adrian Bele[a], Maria Cazacu[a], Carmen Racles[a], Stelian Vlad[a], Mircea Ignat[b]

[a] "Petru Poni" Institute of Macromolecular Chemistry, Aleea Gr. Ghica Voda 41A, Iasi 700487, Romania
[b] National R&D Institute for Electrical Engineering ICPE-CA Bucharest, Splaiul Unirii 313, District 3, Bucharest 030138, Romania

ARTICLE INFO

Article history:
Received 16 March 2015
Received in revised form 30 June 2015
Accepted 5 July 2015
Available online 8 July 2015

Keywords:
A. Ceramics
A. Composites
B. Sol–gel chemistry
C. Differential scanning calorimetry (DSC)
D. Dielectric properties

ABSTRACT

A ceramic material consisting in a zirconium dioxide-lead zirconate mixture has been obtained by precipitation method, its composition being proved by wide angle X-ray powder diffraction and energy-dispersive X-ray spectroscopy. The average diameter of the ceramic particles ranged between 50 and 100 nm, as revealed by transmission electron microscopy images. These were surface treated and used as filler for a high molecular mass polydimethylsiloxane-α,ω-diol (Mn = 450,000) prepared in laboratory, the resulted composites being further processed as films and crosslinked. A condensation procedure, unusual for polydimethylsiloxane having such high molecular mass, with a trifunctional silane was approached for the crosslinking. The effect of filler content on electrical and mechanical properties of the resulted materials was studied and it was found that the dielectric permittivity of nanocomposites increased in line with the concentration of ceramic nanoparticles.

1. Introduction

Silicone rubber is a well-known dielectric elastomer, which can be used for applications such as actuation and for devices able to convert electrical energy into mechanical energy and vice versa [1]. For such applications it is necessary to have a material with low stiffness (low Young's modulus), high breakdown strength and good values for dielectric permittivity [2].

Silicones manifest highly elastic behavior due to the high flexibility of the siloxane bond [3]. While the polarizability of the Si—O bond in polydimethylsiloxane (PDMS) is higher than that of organic nonpolar polymers (e.g., polyethylene), the side methyl groups prevent Si—O dipoles from approaching each other too closely [4], thus the dielectric permittivity of PDMS is very low (ca. 3). Therefore, the siloxanes are chemically modified by attaching polar groups to the silicon atoms, such as *N*-allyl-*N*-methyl-4-nitroaniline [5] or cyanoalkyl [6,7], for the purpose of obtaining large values for the dielectric permittivity.

The incorporation of inorganic fillers with high dielectric permittivity in a polymer matrix is a well-known technique to improve the dielectric constant of the material [8–11] and the use of such fillers sometimes also leads to increasing in mechanical strength. Depending on its type and proportion, the filler can lead to visible changes of the permittivity values of the final material [12].

There are different types of fillers that are generally used for improving the permittivity of the dielectric elastomer: (i) ceramic particles with a high dielectric constant—most used are titanium dioxide, barium titanate, magnesium niobate, lead magnesium niobate-lead titanate, and strontium titanate nanoparticles [13–15]; (ii) conductive particles, such as carbon nanotubes, carbon black, copper–phthalocyanine/polyaniline [16]; (iii) highly polarizable conjugated polymers—undoped poly(3-hexyltiophene), polyaniline, or polythiophene incorporated by blending [10,14,17–21].

In general, commercially available room temperature vulcanization silicone formulations are used to design elastomers for actuators. These are based on low molecular weight polydimethylsiloxane fluid compounds which are converted into silicone elastomers by addition (hydrosilylation) or condensation reactions. Besides siloxanes, there is also a large variety of commercial dielectric elastomer materials available: acrylic VHB foil, polyurethanes, polystyrene/polybutadiene copolymers [22], acrylics and acrylonitrile butadiene rubber [18–21].

In this paper a custom made high molecular weight PDMS was used as polymeric matrix in which different percentages of surface-treated mixed ceramic nanoparticles (MCN) were incorporated. We opted for an interesting ceramic mixture of zirconium dioxide and lead zirconate and used it as filler for the PDMS matrix in order to obtain materials with larger dielectric permittivity. The lead zirconate crystals are orthorhombic antiferroelectric [23,24] with no apparent transitions in the dielectric spectra at low

* Corresponding author. Fax: +40 232 211299.
E-mail address: george.stiubianu@icmpp.ro (G. Stiubianu).

http://dx.doi.org/10.1016/j.materresbull.2015.07.005
0025-5408/

temperatures (<100 °C) and lead zirconate has a value of $\varepsilon_r \sim 160$ at such temperatures. The zirconium dioxide crystals at usual temperatures (<1170 °C) are monoclinic, such as in baddeleyite [25] also with no apparent transitions in the dielectric spectra at low temperatures (<100 °C) and with ε_r value of ~20 at such temperatures. Also zirconium dioxide has the property of stabilizing the permittivity response and it can lower the loss factor value of ceramics [26]. After the incorporation of the MCN filler, the resulted composite materials were processed as films and crosslinked by condensation at room temperature with a trifunctional silane. After the step of aging, the surface, thermal, mechanical and dielectric properties were investigated.

2. Experimental

2.1. Materials and methods

2.1.1. Materials

The reagents for the synthesis of MCN nanoparticles: lead(II) chloride ($PbCl_2$), >99% (Aldrich); zirconium(IV) chloride ($ZrCl_4$), >99.5% (Aldrich); natrium hydroxide (NaOH), pellets, >99% (Fluka AG); urea, >99.0% (Aldrich), all were used as received. Octamethylcyclotetrasiloxane, $[(CH_3)_2SiO]_4$, (D_4), >99% (GC) (Fluka AG) and Pluronic L-31, HO-poly(ethyleneglycol)-*block*-poly(propyleneglycol)-*block*-poly(ethyleneglycol)–OH, M = 1100, $d^{25}{}_{25}$ = 1.02, viscosity (25 °C) = 175 cps (Sigma–Aldrich) were used as received. Methyltriacetoxysilane (MTS) was prepared and purified in house using a technique adapted from literature [27] (>98 %, b.p. = 94–95 °C, $d_4{}^{20}$ = 1.20).

2.1.2. Equipments

Gel permeation chromatography (GPC) measurements for the determination of the molar mass of polydimethylsiloxane were made in $CHCl_3$ on a PL-EMD 950 Chromatograph-Evaporative Mass Detector. The calibration was performed with polystyrene standards.

Dielectric spectroscopy was performed using the Novocontrol "Concept 40" broadband dielectric spectrometer (Hundsangen, Germany) at 25 °C in the frequency range 1–100000 Hz. Water vapors sorption isotherms of the film samples were recorded in dynamic regime by using the fully automated gravimetric analyzer IGAsorp supplied by Hiden Analytical, Warrington (UK). An ultrasensitive microbalance measures the weight change as the humidity is modified in the sample chamber at a constant regulated temperature. The measurement system is controlled by a software package.

Wide angle X-rays diffraction (WAXD) analysis on MCN powder was performed on a Bruker-AXS D8 ADVANCE diffractometer, with Bragg Brentano parafocusing goniometer. Scans were recorded in step mode using Ni-filtered Cu Kα radiation (λ = 0.1541 nm). The working conditions were 40 kV and 30 mA tube power, room temperature. The Bruker computer softwares Eva 11 and Topaz 3.1 were used to plot and process the data.

Differential scanning calorimetry (DSC) measurements were conducted with a DSC 200 F3 Maia (Netzsch, Germany). About 10 mg of sample was heated in pressed and punched aluminum crucibles at a heating rate of 10 °C min^{-1}, in nitrogen inert atmosphere. The temperature range for TG–DTG measurements performed with the same instrument was 25–750 °C with a heating rate of 10 °C min^{-1}.

An Energy Dispersive X-Ray system (EDX) available on environmental scanning electron microscope (ESEM) type Quanta 200 was used for qualitative analysis and elemental mapping. The transmission electron microscopy (TEM) images were taken using a dedicated HITACHI HT7700 microscope operated in high contrast mode at 100 kV accelerating voltage. The samples have been prepared by placing small droplets of the diluted dispersion (1 g/L) of ceramic powder on 300 mesh carbon coated copper grids and dried in vacuum at 50 °C.

Stress–strain measurements were performed on a TIRA test 2161 apparatus, Maschinenbau GmbH Ravenstein, Germany on dumbbell-shaped cut samples with dimensions of 50 × 8.5 × 4 mm. Measurements were run at an extension rate of 20 mm/min, at room temperature. All samples were measured three times and the averages of the obtained values were taken into consideration. The acquired data were processed with MatLab software. Cyclic tensile stress tests were performed on the similar samples between 2 and 100% strain. The maximum force applied was tensile stress value as determined by previous test. Five stretch/recovery cycles were registered. The stationary time at minimum and maximum applied stress was 2 s.

Dielectric strength measurements were made on a home-made installation (PERCRO Laboratory–TeCIP Institute–Scuola Superiore Sant'Anna, Pisa, Italy) consisting in high-speed high-voltage power amplifier, function generator, and an oscilloscope. The brass electrodes were applied on the film samples and the measurements were performed at 60 Hz, and a voltage increase rate of 2000 V s^{-1} at room temperature (25 °C). The samples were previously brought into equilibrium with the humidity of the environment in which the measurements were made. Three samples were analyzed for each composite formulation and the lowest value was taken into consideration.

A home-made set-up was used for performing energy harvesting tests with the new dielectric elastomers (Fig. 1ESI). In this set-up electrodes (20 × 20 mm) made of copper plated textolite were placed on each side of the sample and the voltage was recorded with a memory oscilloscope Tektronix DPO 4032 with two channels, at frequency of 100 MHz. The kinetics consists in a steel ball (m = 7.1 g) falling freely from a height of 100 mm in the center of the upper electrode surface. The signal wave shape and the voltage levels corresponding for the peaks at the impact of the ball on contact surface of the sensor were monitored and were acquired (Fig. 2ESI). Three measurements were performed for each sample and the average values were taken into account.

2.2. Procedure

2.2.1. Preparation of mixed ceramics nanoparticles, MCN

The MCN nanoparticles were prepared by using the procedure described by Oren et al. [28], namely a homogeneous precipitation, modified as follows. First a mixture of 100 mL of cation stock solutions was prepared by mixing lead and zirconium chlorides (0.556 g $PbCl_2$ and 4.66 g $ZrCl_4$) in a glass beaker at room temperature (RT) (Fig. 1). Then a solution of urea (15.5 g urea in

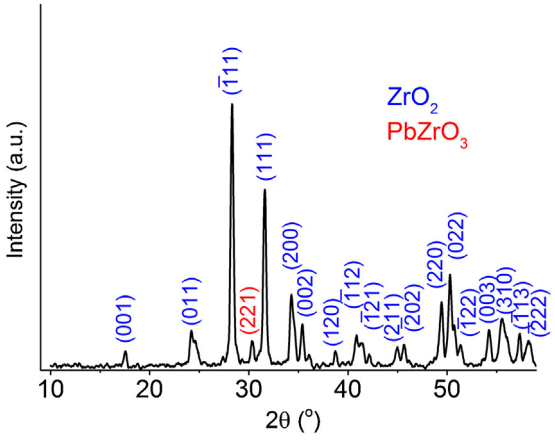

Fig. 1. XRD patterns of the MCN powder (2-column fitting image).

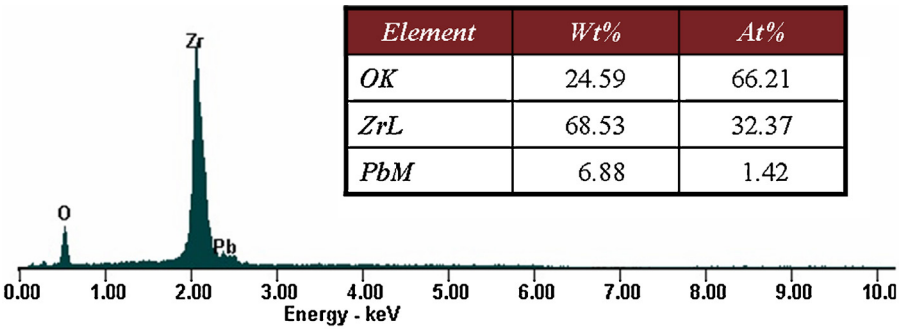

Element	Wt%	At%
OK	24.59	66.21
ZrL	68.53	32.37
PbM	6.88	1.42

Fig. 2. EDX data for MCN (single column fitting image).

220 ml distilled water) was mixed with the cation stock solution, leading to a clear solution that was further heated at 90 °C on a hot plate for ~2 h. A solution of sodium hydroxide (50 ml, 2 M) was added and, under continuous heating, the precipitation started in ~10 min, when turbidity appeared in the clear solution. Precipitates were aged for 1 h at 90–95 °C without stirring. Afterwards, the precipitates were separated by centrifugal filtration at 6000 rpm and the recovered material was washed with distilled water twice by centrifugation. The resulted material was oven-dried at 90 °C for 2 h followed by calcination, the temperature being raised (with 10 °C/min) up to 700 °C and maintained for 5 h.

2.2.2. Preparation of high molecular mass polydimethylsiloxane-α,ω-diol

PDMS (polydimethylsiloxane-α,ω-diol) was synthesized according to an already described procedure [29,30]: polymerization in bulk of octamethylcyclotetrasiloxane in presence of H_2SO_4, at room temperature. The polymer was purified by successive washings with neutral–slightly alkaline solution and then with distilled water. The washed polymer was devolatilized under vacuum at 170–180 °C in order to remove both water and low molecular weight siloxanes. The gel permeation chromatographic analysis (GPC) of the pure polymer was carried out, with $CHCl_3$ as eluent. The number average molecular mass was determined as being 450,000, with polydispersity index ($I = M_w/M_n$) of 1.4.

2.2.3. Surface treatment of the filler

An well established amount of MCN was immersed in surfactant, Pluronic L-31, and the mixture was ultrasonicated for 30 min in a Hielscher Ultrasonic Processor UTR 200, followed by filtration of excess surfactant.

2.2.4. Preparation of the silicone-MCN composites and film formation

The PDMS was quickly mixed with treated dielectric material powder (MCN) and the crosslinking agent (MTS) in amounts showed in Table 1, by mechanical stirring. After a uniform mixture was formed, it has been deaerated in vacuo and cast in Teflon mold where it was allowed to crosslink and aged for two weeks in normal conditions, the atmospheric moisture being the hydrolysis agent for methyltriacetoxysilane as crosslinker. The dielectric elastomer films were then manually peeled off from the surface of the mold.

Table 1
The used recipes for the preparation of the composite films.

Sample	Reagent (mass relative to PDMS)		
	PDMS	MCN	MTS
S1	100	0	5
S2	100	2	5
S3	100	6.5	5

3. Results and discussion

A procedure reported in literature [28] was adapted to obtain a ceramic material based on lead and zirconium, being known that such materials have high dielectric permittivity [23–26]. The obtained ceramic material, MCN, was first analyzed by X-Ray Powder Diffraction. The presence of diffraction peaks (Fig. 1) proves the crystalline nature of MCN. These are specific for zirconium dioxide and lead zirconate and were identified by comparison with the XRD spectra reported by different authors [24,31–33].

The peaks at 2θ angles of 24.44° (0 1 1), 28.17° ($\bar{1}$ 1 1), 31.7° (1 1 1), 34.3° (2 0 0), 35.4° (0 0 2) and 49.3° (2 2 0) and 50.2° (0 2 2) are specific to zirconium dioxide. The peaks at 30.4° (0 4 0) and 30.6° (2 2 1) are specific for lead zirconate. By measuring the ratio of the most intense peaks at 28.17° for zirconium dioxide and at 30.6° for lead zirconate, it can be concluded that the ratio of zirconium dioxide to lead zirconate in the nanoparticles is 100:12, in a reasonable agreement with EDX data from which a ratio of 100:13 was calculated (Fig. 2).

TEM image (Fig. 3) shows the formation of nanoparticles with average diameters of 74 nm. The electron diffraction confirms the crystalline structure of the synthesized MCN.

The MCN powder was used as filler for polydimethylsiloxane elastomer films, with the purpose of improving their dielectric properties, while simultaneously trying to preserve in the final composites the softness and the high stretch capability specific for pure PDMS films. Two composites, with 2.0 and 6.5% MCN reported to the PDMS mass, were prepared (Table 1). The curing of the composites was performed after their processing in film, when slow hydrolysis of MTS occurs in the presence of environmental humidity, and condensation of the resulted triol with the Si–OH chain ends leads to the network formation. Acetic acid formed as a MTS hydrolysis byproduct migrates out of the film during the aging process. A free standing, elastic, robust film is formed, which is pelled off and further investigated.

The stress–strain tests (Fig. 4a, Table 2) reveal that the composites containing ceramic nanoparticles have lower elongation at break compared to pristine PDMS film, i.e. ca. 860% and 600% respectively, versus 2200%. However, the values for the elongation at break are still high, which is a prerequisite for these materials to be suitable for use as dielectric elastomers. The breaking stress values for the nanocomposites are slightly lower compared with the reference sample S1, but they are characteristic for soft materials. This behavior could be explained judging the surface of the nanoparticles and aggregated nanoparticles as stress concentrator. Also, the presence of nanoparticles introduces defects in the PDMS polymeric network.

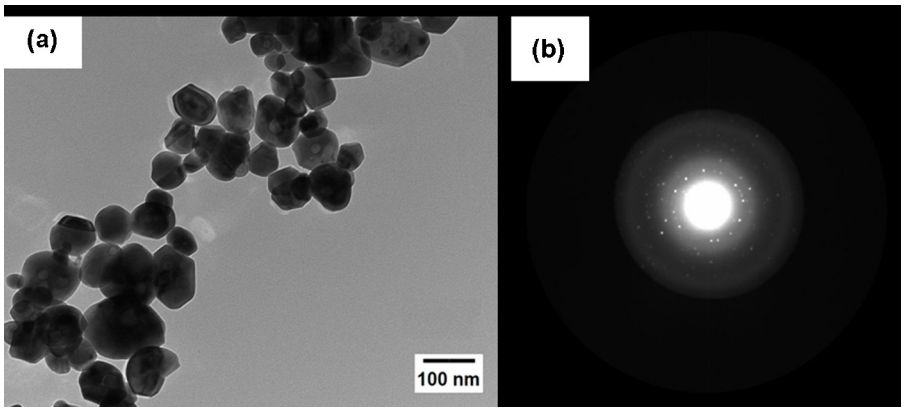

Fig. 3. TEM analysis of the MCN: (a) image of the nanoparticles; (b) electron diffraction of the nanoparticles (2-column fitting image).

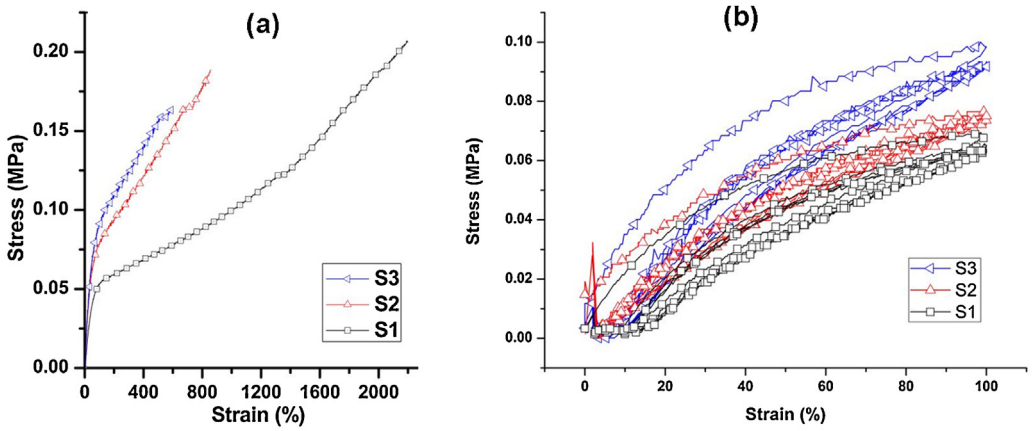

Fig. 4. (a) Stress–strain curves for elastomer films containing nanoparticles; (b) Cyclic stress–strain films for elastomers with MCN nanoparticles (2-column fitting image).

Table 2
Absorbed and released energy (KJ/m^3) calculated at 100% elongation for five cycles.

Cycles	S1			S2			S3		
	loading	unloading	Hist., %	loading	unloading	Hist., %	loading	unloading	Hist., %
1	0.506	−0.357	29.44	0.555	−0.426	23.24	0.723	−0.528	26.97
2	0.407	−0.333	18.18	0.462	−0.408	11.67	0.583	−0.495	15.09
3	0.390	−0.323	17.17	0.451	−0.407	9.75	0.565	−0.489	13.45
4	0.382	−0.321	15.97	0.457	−0.417	8.75	0.560	−0.493	11.96
5	0.380	−0.323	15.00	0.469	−0.428	8.74	0.563	−0.501	11.01

The Young's modulus showed a slight increase with the MCN content, which is normal, given the ceramic nature of the filler, which acts as a reinforcing agent for the PDMS matrix.

The value of the stress at a certain strain for these samples is larger than the corresponding value for the reference sample with pure PDMS (S1), as the presence of nanoparticles improves the initial elastic character of the polydimethylsiloxane matrix, while the sample S1 has a viscous component of deformation after the initial 50% strain. The composite films have small hysteresis loops at cyclic stress–strain (Fig. 4b), making these suitable for use in flexible devices, like. The cyclic stress–strain curves show some hysteresis loop, higher in the first cycle (up to 30%), after which they are reduced (between 9 and 15%) and stabilize (Fig. 4b, Table 2). From cyclic stress–strain curves, it can calculate the tensile toughness. This parameter represents the amount of energy per volume that material can absorb before failure or at a predetermined elongation (in this case 100%) and was estimated as area of loading–unloading curve for each cycle. The toughness at 100% elongation was determined on the cyclic stress–strain curves of the original samples as an indirect measure of the energy that the elastic material could release when force that acted on it was removed like in a harvesting energy system (Table 2). As expected, it can be seen that this value increases by incorporating MCN and enhancing their amount, for example, from 0.506 for S1–0.555 for sample S2 and 0.723 KJ/m^3 for sample S3 in first cycle read on the loading branch. In the fifth cycle, these are all lower but keeps the same hierarchy (0.380 for S1, 0.469 for S2 and 0.563 KJ/m^3 for S3). As a result of the viscoelastic loss, the energies released on the return branch are lower. This loss is lower in the filled samples, in special in the case of sample S2, as compared with reference sample S1.

The dielectric permittivity (ε') and loss (ε'') were recorded in the frequency domain of six decades (log scale) of frequency, i.e. 1–100000 Hz, at constant temperature of 25 °C. Samples having uniform thickness in the 0.27–0.77 mm range were placed

between gold plated round electrodes, the upper electrode having a 20 mm diameter.

When the ceramic nanoparticles are introduced in the composition of the films, the value of the dielectric permittivity increases – with up to 26% for the sample S3 (4.35) compared with reference S1 (3.20) (Fig. 5a) at 1 Hz, this increase being expected one.

The electrostatic polarization leads to the field-induced polarization of the dispersed phase relative to the continuous phase. When an electric voltage is applied, positive and negative charges appear at the surface of the particles. Each particle can be described as a dipole, the particles align head-to-tail in the direction of the electric field and polarization leads to increased capability of the prepared dielectric materials to store energy [34]. There are several theoretical approaches used for predicting the values of effective dielectric constant of polymer composite systems. The simplest method is the volume-fraction average:

$$\varepsilon_{ff} = \varphi_p \varepsilon_p + \varphi_c \varepsilon_c \quad (1)$$

where the subscripts p and c are the polymer and the ceramic phase, respectively, and φ is the volume fraction of the constituents. This model (Eq. (1)) predicts a sharp increase of the effective dielectric constant starting at a low volume fraction of the ceramic filler. However this prediction has been disproved by both theoretical [35] and experimental studies [36].

The Maxwell–Garnett equation has been developed as a mean to approach the calculated theoretical and the practical results and it is an approximation of a single spherical inclusion surrounded by a continuous matrix of the polymer [37]. However this model is representative at very low (close to zero) concentrations of filler:

$$\varepsilon_{ff} = \varepsilon_p \times \left[\frac{\varepsilon_c + 2\varepsilon_p - 2(1-\varphi_p)(\varepsilon_p - \varepsilon_c)}{\varepsilon_c - 2\varepsilon_p + (1-\varphi_p)(\varepsilon_p - \varepsilon_c)}\right] \quad (2)$$

In the Bruggeman model the binary mixture is made of repeated units cells, each consisting of the polymer matrix which has spherical inclusions in the center [37]. The effective dielectric constant calculated with the Bruggeman equation increases sharply for filler volume fractions above 20%. The effective dielectric constant (ε_{ff}) of the composite mixture is given by:

$$\varphi_p \left[\frac{\varepsilon_p - \varepsilon_{eff}}{\varepsilon_1 + 2\varepsilon_{eff}}\right] + \varphi_c \left[\frac{\varepsilon_c - \varepsilon_{eff}}{\varepsilon_c + 2\varepsilon_{eff}}\right] = 0 \quad (3)$$

The two-component power-law model for complex permittivity is used for such calculations in different systems, such as air-particulate composites [38], ceramic–ceramic composites [39] and polymer–ceramic composites [40]. In this model, the effective permittivity of two-component systems is determined by introducing the volume fraction of each component according to Eq. (4):

$$\varepsilon_{ff}{}^{\beta} = \varphi_c \varepsilon_c{}^{\beta} + (1-\varphi_c)\varepsilon_p{}^{\beta} \quad (4)$$

β is a dimensionless parameter and its value is determined by the shape and orientation of the filler particles within the bulk composite [41] and can take values between 1 and −1. For randomly oriented ellipsoids Landau, Lifshitz [42] and Looyenga [43] determined that $\beta = 1/3$.

Fig. 6 shows the values for the dielectric permittivity of the samples as resulted from the above formulas and can be easily compared with the experimental values. The values for $\varepsilon_p = 3.2$ and $\varepsilon_c = 19.9$ and the volume fractions $\varphi_p = 1$ and $\varphi_c = 0$ for S1, $\varphi_p = 0.98$ and $\varphi_c = 0.02$ for S2, and $\varphi_p = 0.938$ and $\varphi_c = 0.062$ for S3 were considered.

It can be seen (Fig. 6) that the dielectric responses at 1 Hz of ceramic–polymer systems can be best described by the volume fraction average rule.

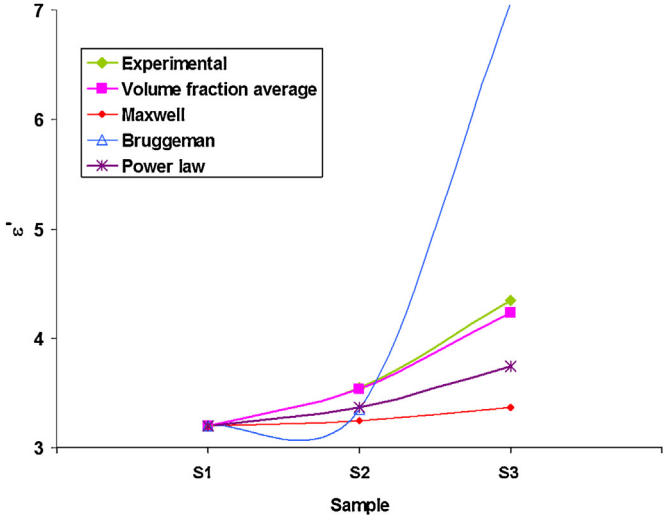

Fig. 6. The values of the dielectric constant for the samples as determined experimentally in comparison with the values calculated with equations of different models.

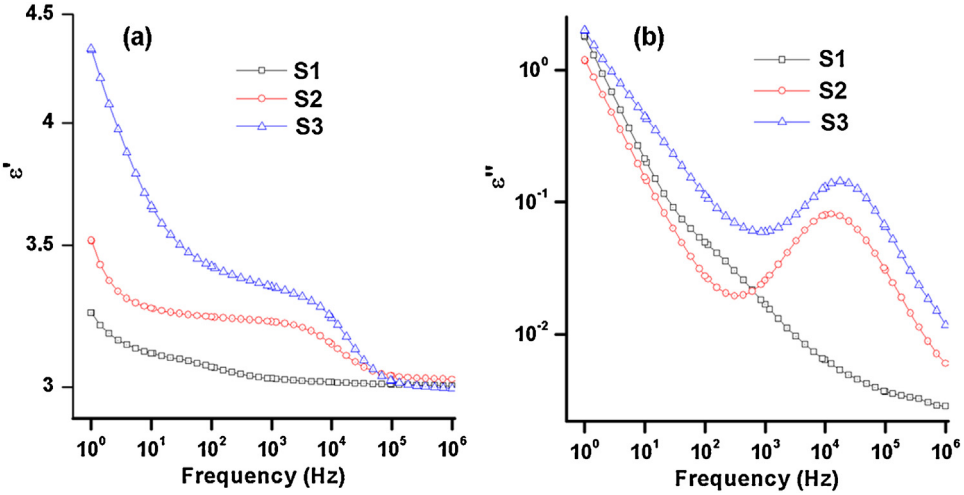

Fig. 5. (a) The variation of dielectric constant (ε') with frequency for elastomers with MCN; (b) The variation of dielectric loss (ε'') with frequency for elastomers with MCN (2-column fitting image).

There is a relaxation at higher frequencies (5×10^3 Hz) due to charge accumulation at the interface between the nanoparticle surface and the polymer matrix, and this relaxation is also visible in the variation of the loss factor when sweeping the frequency (Fig. 5b). The loss factor maintains low values when the nanoparticles are introduced in the polymer matrix (Fig. 5b). The ε' values of the films decrease with increasing frequency. A drop in ε' occurs when the frequency reaches 10^4 Hz since the dipole relaxation in the composite films lags behind the change of applied field. The characteristic relaxation peaks of the polysiloxane matrix in ε'' curves are not present in the composites due to the presence of nanoparticles, which leads to decreasing of the free volume in the polymer matrix and increasing the density of polar groups [44]. Increased values of permittivity were registered as the free volume between PDMS chains decreases, but this has the unwanted effect of significantly smaller strain values for the films as shown in the results from the stress–strain tests, and such a behavior was recorded before for other siloxane-based films [45].

Unexpectedly, the pure crosslinked PDMS (S1) shows a low enough value for electric breakdown field (EBD) of 28.6 kV/mm (Table 3). This could be explained by the low crosslinking degree of very long and flexible chains which allows keeping a high free volume in material. The small air-filled voids, left by late removing of condensation by-products, which elongate in the direction of the field until breakdown occurs [46] could also contribute to the lowering of this parameter's value. As a result, by adding high dielectric ceramic material, the decreasing of EBD value as compared with that of matrix S1 is not as would be expected since it is partially compensated by reducing the effect of free volume in the matrix as a result of nanoparticles incorporation.

DSC experiments (Fig.7) highlight the glass transition around −124 °C, an exothermic peak at about −70/−72 °C and an endothermic peak at −38/−39 °C, assigned to the phenomenon of cold crystallization and to the melting of the crystalline phase, respectively. The peak corresponding to melting (−38 °C) is similar in surface with the one corresponding for crystallization (−70 °C) (values for ΔH between 21...24 J/g) and this indicates that a significant amount of crystalline phase develops during the cooling scan. The DSC curves of samples S2 and S3 are very similar with those of S1. This behavior suggests the ceramic particles have negligible influence on the thermal behavior of the samples.

When materials are designed for use in electronic devices, it is convenient to have an elastomer with stable operation and therefore the numerical values for characteristics of interest must be stable in different conditions of moisture and temperature. An increase in the moisture sorption capacity with the rising content of ceramic nanoparticles was registered by DVS analysis, as can be seen in Fig. 8 (from 0.45 % in pure crosslinked PDMS to 1.35% in the material with 6.5% MCN). This is due to the capacity of the ceramic material to adsorb water on their surface. However, the effect is diminished due to the well-known hydrophobicity of the PDMS matrix. The maximum sorption capacity obtained in this case is comparable with the ones obtained for other materials used as dielectric elastomers such as acrylic rubber 3 M VHB (1.3%) [47]. The sorption isotherms correspond to a type V material and show that the dielectric elastomer films are hydrophobic materials with low porosity and present weak interactions between sorbed and sorbent materials. From the kinetic curves (not shown) it was determined that the rate of desorption of water vapors is slower than the sorption rate, leading to appearance of a hysteresis loop.

The average values for the diffusion coefficient (D) at short and long times (Table ESI1), estimated according to procedure established in literature [48,49] slightly decrease as a result of the incorporation of the MCN within the silicone matrix, from $5.62\,10^{-7}$ (S1)–$1.34{\cdot}10^{-7}$ cm^2/s (S3). This could be due to the decrease in mobility, within hydrophobe silicone matrix, of water due to its tendency to be retented by more hydrophilic filler particles. A decreasing of one magnitude order of the diffusion coefficient was obtained for all samples at $t = \infty$ (corresponding to sorption equilibrium), $5.29\,10^{-8}$ (S1), $4.29\,10^{-8}$ (S2) and $2.49\,10^{-8}$ cm^2/s (S3).

The electromechanical (actuation and energy harvesting) abilities of the materials are mainly determined by the values of Young modulus (Y) which is desired to be low and dielectric permittivity (ε') and dielectric strength (EBD) which should be as high. In our case, only a slight increase was registered in dielectric permittivity, the last two parameters showing evolutions inverse than would be required (Table 3).

The energy output, E, of dielectric elastomers can be estimated based on the mechanical and electrical properties of tested samples [50]. The capacitance of a parallel-plane capacitor can be calculated as such:

$$C = \varepsilon_0 \varepsilon\prime (A \times z) = \varepsilon_0 \varepsilon\prime (v/z^2) \quad (5)$$

where ε' is the permittivity, z—thickness of the sample and A—effective area of the sample. The second equality in this equation is due to the constant volume of the elastomer ($A\,z = v$ = volume, which is constant). The energy that can be gained from a cycle of operation (consists of one stretch and one relaxation of the variable generator) depends on the difference between the total capacitance in stretched state, C_2, and relaxed state, C_1, and the square of the applied voltage, V:

$$E = 0.5 C_2 V^2 \left[\left(\frac{C_2}{C_1} \right) - 1 \right] \quad (6)$$

If there is a constant charge, Q, over a short period of time, the voltages in stretched state, V_1, and relaxed state, V_2, can be expressed:

$$V = \frac{Q}{C} \rightarrow V_1 = \frac{Q}{C_1} = \left(\frac{C_2}{C_1} \right) \left(\frac{Q}{C_2} \right) = \left(\frac{C_2}{C_1} \right) V_2 \quad (7)$$

For samples with 5 cm in length, a constant width of 2 cm, a known measured thickness (z_1) and a maximum strain determined from mechanical tests, the energy output from a uniaxial deformation was calculated (Table 3–E <J>). It can be noticed that when the content of MCN in the sample increases, there are significant improvements of the theoretical energy output of the sample.

Table 3
The main mechanical and dielectric characteristics of the silicone composites.

Sample	Breaking stress, MPa	Elongation at break, %	Young's modulus[a], MPa^{-1}	ε' (10 Hz)	ε'' (10 Hz)	EBD, kV/mm	E[b], J	Upp[c], V/mm
S1	0.206	2198	0.00093	3.11	0.211	28.6	0.53	7.0
S2	0.188	858	0.00165	3.26	0.153	30.1	2.19	7.3
S3	0.164	592	0.00185	3.65	0.446	11.9	3.74	16.7

[a] Calculated at 15% elongation;
[b] Theoretical estimated energy output;
[c] Harvested voltage measured peak to peak and reported to film thickness.

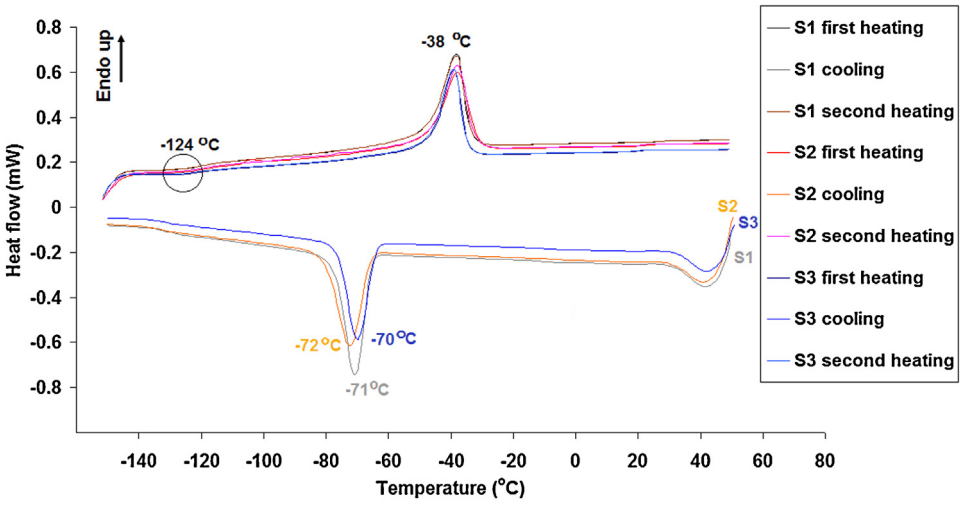

Fig. 7. The differential scanning calorimetry curves for elastomers with MCN (2-column fitting image).

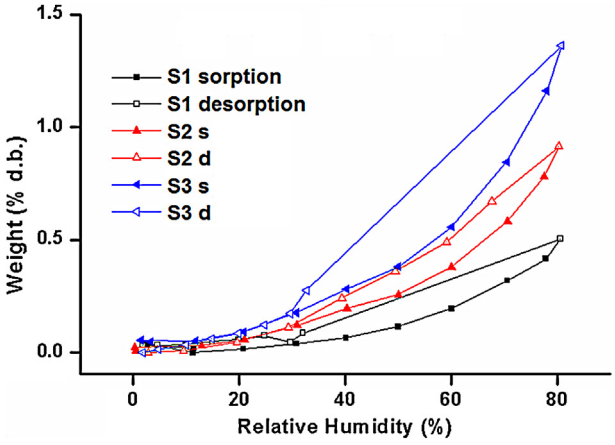

Fig. 8. Dynamic vapor sorption isotherms for the elastomers containing ceramic nanoparticles.

Energy harvesting experiments were performed as follows. A mechanical microimpulse by the fall of a microball (m = 7.1 g) from a set height (h = 0.1 m) was applied to the sample and the resulting voltage spike was used to estimate the ability of the elastomer to convert the mechanical energy into electrical one [30]. The dynamic parameters used for these experiments were as follows:

- speed at contact with the elastomeric membrane, υ = 1.4 m/s;
- mechanical impulse, $p = 9.94\,10^{-3}$ [Ns];
- kinetic energy in contact, $E = 6.96\,10^{-3}$ [J];
- the micro-force, F = 0.0696 [N].

Three measurements were made for each sample and the average value of the results was taken into account (Table ESI1). Since the film thicknesses of the three samples were different, voltage values recorded were reported to this in order to be able to compare the results to each other. Only a very slight increase in voltage/mm, measured peak to peak (Upp), was recorded for sample S2 containing 2.0 wt% MCN (7.3 V/mm) toward the reference sample S1 (7.0 V/mm), while by increasing the amount of added MCN at 6.5 wt% in the case of sample S3, the amount of energy harvested was more than double (16.7 V/mm) (Fig. ESI2). Although the calculated values for energy output and experimental harvested voltages are expressed in different ways, they follow the same trend increasing as filler amount enriches.

4. Conclusion

A new type of mixed ceramics nanoparticles was obtained using a chemical precipitation method and incorporated in two different weight percentages (2 and 6.5 wt%) in a high molecular mass polydimethylsiloxane-α,ω-diol subsequently crosslinked with methyltriacetoxysilane. When compared with elastomers made with pure PDMS, a decrease of the maximum strain for elastomers with MCN was observed, however the value for the strain remained very large. Small water sorption values were registered for elastomers incorporating MCN filler, this indicating that the hydrophobic character of the polydimethylsiloxane is preserved. The value of dielectric constant increases with the increase in the content of dielectric ceramic, improving the dielectric behavior. The dielectric responses at 1 Hz of ceramic–polymer systems are best described by the volume fraction average rule. The nanocomposite dielectric elastomer films have small hysteresis loops at cyclic stress–strain, which recommend them for use in flexible piezoelectric devices. The dielectric loss at small frequencies (< 10 Hz) is similar for all films – the nanoparticles do not lead to increase of dielectric losses. The calculated energy output from a uniaxial deformation of the dielectric elastomer films improves significantly when the content of MCN in the films increases, making these films suitable for use in energy harvesting. The energy harvesting ability measured in a microball fall experiment confirmed this tendency.

Acknowledgements

The work presented in this paper is developed in the context of the project PolyWEC (www.polywec.org, prj. ref. 309139), a FET-Energy project that is partially funded by the 7th Framework Programme of European Community and co-financed by UEFISCDI (Contract 205EU).

Appendix A. Supplementary data

Supplementary data associated with this article can be found, in the online version, at http://dx.doi.org/10.1016/j.materresbull.2015.07.005.

References

[1] N. Gharavi, M. Razzaghi-Kashani, N. Golshan-Ebrahimi, Effect of organo-clay on the dielectric relaxation response of silicone rubber, Smart Mater. Struct. 19 (2) (2010) 025002, doi:http://dx.doi.org/10.1088/0964-1726/19/2/025002.

[2] T. Enis, I. Sauers, Industrial applications perspective of nanodielectrics, in: J. Nelson Keith (Ed.), Dielectric Polymer Nanocomposites, Springer, New York, NY, USA, 2009, doi:http://dx.doi.org/10.1007/978-1-4419-1591-7_11 pp. 321, Chapter 11.

[3] S. Koulouridis, G. Kiziltas, Y. Zhou, D.J. Hansford, J.L. Volakis, Polymer–ceramic composites for microwave applications: fabrication and performance assessment, IEEE Trans. Microw. Theory 54 (2006) 4202–4208, doi:http://dx.doi.org/10.1109/TMTT.2006.885887.

[4] F. Gubbels, R. De Jaeger, M. Gleria, Silicones in industrial applications, in: R. De Jaeger, M. Gleria (Eds.), Inorganic Polymers, Nova Science Publishers, 2007, 2015, pp. 61–162 Chapter 2.

[5] S. Risse, B. Kussmaul, H. Krüger, R. Waché, G. Kofod, DEA material enhancement with dipole grafting PDMS network, Proc. SPIE 7976, Electroactive Polymer Actuators and Devices (EAPAD) 2011, 79760N. http://dx.doi.org/10.1117/12.881919.

[6] B. Risse, H. Krüger, G. Kofod, Synergistic improvement of actuation properties with compatibilized high permittivity filler, Adv. Funct. Mater. 22 (2012) 3958–3962, doi:http://dx.doi.org/10.1002/adfm.201200320.

[7] C. Racles, M. Cazacu, B. Fischer, D.M. Opris, Synthesis and characterization of silicones containing cyanopropyl groups and their use in dielectric elastomer actuators, Smart Mater. Struct. 22 (2013) , doi:http://dx.doi.org/10.1088/0964-1726/22/10/104004 (10 pages).

[8] G. Momen, M. Farzaneh, Survey of micro/nano filler use to improve silicone rubber for outdoor insulators, Rev. Adv. Mater. Sci. 27 (2011) 1–13.

[9] D. Khastgir, K. Adachi, Rheological and dielectric studies of aggregation of barium titanate particles suspended in polydimethylsiloxane, Polymer 41 (2000) 6403–6413, doi:http://dx.doi.org/10.1016/S0032-3861(99) 840-X.

[10] F. Carpi, G. Gallone, F. Galantini, D. De Rossi, Enhancing the dielectric permittivity of elastomers, in: F. Carpi, D. De Rossi, R. Kornbluh, R. Pelrine, P. Sommer-Larsen (Eds.), Dielectric Elastomers as Electromechanical Transducers: Fundamentals, Materials, Devices, Models and Applications of an emerging electroactive Polymer Technology, Elsevier Ltd., 2008, 2015 pp. 60, Chapter 6.

[11] G. Gallone, F. Carpi, D. De Rossi, G. Levita, A. Marchetti, Dielectric constant enhancement in a silicone elastomer filled with lead magnesium niobate–lead titanate, Mater. Sci. Eng. C 27 (2007) 110–116, doi:http://dx.doi.org/10.1016/j.msec.2006.03.003.

[12] A.A. Babar, V.A. Bhagavati, L. Ukkonen, A.Z. Elsherbeni, P. Kallio, L. Sydänheimo, Performance of high-permittivity ceramic–polymer composite as a substrate for UHF RFID tag antennas, Int. J. Antennas Propag. (2012) 8, doi:http://dx.doi.org/10.1155/2012/905409 Article ID 90540.

[13] Z. Wang, J.K. Nelson, J. Miao, R.J. Linhardt, L.S. Schadler, H. Hillborg, Su Zhao, Effect of high aspect ratio filler on dielectric properties of polymer composites: a study on barium titanate fibers and graphene platelets, IEEE Trans. Dielectr. Electr. Insul. 19 (2012) 960–967, doi:http://dx.doi.org/10.1109/TDEI.2012.6215100.

[14] Yansheng Yin, Xueting Chang, Ocean engineering application of nanocomposites, in: Jingsong Leng, Alan K.T. Lau (Eds.), Multifunctional Polymer Nanocomposites, CRC Press, Taylor and Francis Group, Boca Raton, FL, 2011, pp. 423–439, doi:http://dx.doi.org/10.1201/b10462-11 Chapter 10.

[15] M.T. Sebastian, H. Jantunen, Polymer–ceramic composites of 0–3 connectivity for circuits in electronics: a review, Int. J. Appl. Ceram. Technol. 7 (2010) 415–434, doi:http://dx.doi.org/10.1111/j.1744-7402.2009.02482.x.

[16] C. Huang, Q.M. Zhang, Fully functionalized high dielectric constant nanophase polymers with high electromechanical response, Adv. Mater. 17 (2005) 1153–1158, doi:http://dx.doi.org/10.1002/adma.200401161.

[17] D.M. Opris, M. Molberg, C. Walder, Y.S. Ko, B. Fischer, F.A. Nüesch, New silicone composites for dielectric elastomer actuator applications in competition with acrylic foil, Adv. Funct. Mater. 21 (18) (2011) 3531–3539, doi:http://dx.doi.org/10.1002/adfm.201101039.

[18] Hang Zhao, Dong-Rui Wang, Jun-Wei Zha, Jun Zhao, Zhi-Min Dang, Increased electroaction through a molecular flexibility tuning process in TiO_2–polydimethylsilicone nanocomposites, J. Mater. Chem. A 1 (2013) 3140–3145, doi:http://dx.doi.org/10.1039/C2TA01026G.

[19] Y. Zhou, J. Wang, H. Chen, Q. Nie, Q. Sun, Y. Wang, The influence of pre-stressing on breakdown characteristics in liquid silicone rubber, J. Electrostat. 67 (2009) 422–425, doi:http://dx.doi.org/10.1016/j.elstat.2009.01.029.

[20] R.J. Spontak, R. Shankar, T.K. Ghosh, Electroactive nanostructured polymers as tunable actuators, Adv. Mater. 19 (2007) 2218–2223, doi:http://dx.doi.org/10.1002/adma.200602644.

[21] H. Zhang, L. Düring, G. Kovacs, W. Yuan, X. Niu, Q. Pei, Interpenetrating polymer networks based on acrylic elastomers and plasticizers with improved actuation temperature range, Polym. Int. 59 (2010) 384–390, doi:http://dx.doi.org/10.1002/pi.2784.

[22] P. Brochu, Q. Pei, Advances in dielectric elastomers for actuators and artificial muscles, Macromol. Rapid Commun. 31 (2010) 10–36, doi:http://dx.doi.org/10.1002/marc.200900425.

[23] G. Shirane, E. Sawaguchi, Y. Takagi, Dielectric properties of lead zirconate, Phys. Rev. 84 (3) (1951) 476–481.

[24] Sukkha Usa, Muanghlua Rangson, Niemcharoen Surasak, Boonchoma Banjong, Vittayakorn Naratip, Antiferroelectric–ferroelectric phase transition in lead zinc niobate modified lead zirconate ceramics: crystal studies, microstructure, thermal and electrical properties, Appl. Phys. A 100 (2010) 551–559, doi:http://dx.doi.org/10.1007/s00339-010-5871-1.

[25] R.H. Nielsen, G. Wilfing, Zirconium and zirconium compounds, Ullmann's Encyclopedia of Industrial Chemistry, Wiley-VCH, Weinheim, 2005, doi:http://dx.doi.org/10.1002/0471238961.26091803.a01.pub2 Chapter Zirconium and Zirconium Compounds.

[26] T.R. Armstrong, L.E. Morgens, A.K. Maurice, R.C. Buchanan, Effects of zirconia on microstructure and dielectric properties of barium titanate ceramics, J. Am. Ceram. Soc. 72 (4) (1989) 605–611, doi:http://dx.doi.org/10.1111/j.1151-2916.1989.tb06182.x.

[27] K.A. Andrianov, A.A. Zhdanov, A.A. Bogdanova, Reaction of alkylacetoxysilanes with alcohols, Dokl. Akad. Nauk SSSR 94 (1954) 697–699.

[28] E.E. Oren, E. Taspinar, A.C. Tas, Preparation of lead zirconate by homogeneous precipitation and calcination, J. Am. Ceram. Soc. 80 (10) (1997) 2714–2716, doi:http://dx.doi.org/10.1111/j.1151-2916.1997.tb03181.x.

[29] M. Cazacu, M. Antohi, C. Racles, A. Vlad, N. Forna, Silicone-based composite for lining of removable dental prosthesis, J. Compos. Mater. 43 (19) (2009) 2045–2055, doi:http://dx.doi.org/10.1177/0021998309340447.

[30] M. Cazacu, M. Ignat, C. Racles, M. Cristea, V. Musteata, D. Ovezea, D. Lipcinski, Well-defined silicone–titania composites with good performances in actuation and energy harvesting, J. Compos. Mater. 48 (13) (2014) 1533–1545, doi:http://dx.doi.org/10.1177/0021998313488148.

[31] L.B. Kong, J. Ma, W. Zhu, O.K. Tan, Preparation and characterization of lead zirconate ceramics from high-energy ball milled powder, Mater. Lett. 49 (2001) 96–101, doi:http://dx.doi.org/10.1016/S0167-577X(00) 350-5.

[32] H. McMurdie, M.C. Morris, E.H. Evans, B. Paretzkin, W. Wong-Ng, Standard X-ray diffraction powder patterns from the jcpds research associateship, Powder Diffr. 1 (3) (1986) 265–275.

[33] I. Flavia Princess Nesamani, V. Lakshmi Prabha, P. Aswathy, D. Nirmal, Synthesis and dielectric studies of monoclinic nanosized zirconia, Adv. Cond. Matter Phys. 828492 (2014) 7.

[34] Jiongxin Lu, C.P. Wong, Nanoparticle-based high-k dielectric composites: opportunities and challenges, in: J.E. Morris (Ed.), Nanopackaging: Nanotechnologies and Electronics Packaging, Springer Science + Business Media, LLC, 2008, pp. 121–137 Chapter 7.

[35] K.L. Ying, T.E. Hsieh, Sintering behaviors and dielectric properties of nanocrystalline barium titanate, Mater. Sci. Eng. B: Sol. State Mater. Adv. Technol. 138 (2007) 241–245.

[36] C. Brosseau, Modeling and simulation of dielectric heterostructures: a physical survey from an historical perspective, J. Phys. D: Appl. Phys. 39 (2006) 1277–1294.

[37] D.-H. Yoon, J. Zhang, B.I. Lee, Dielectric constant and mixing model of barium titanate composite thick films, Mater. Res. Bull. 38 (2003) 765–772.

[38] S.O. Nelson, Observations on the density dependence of dielectric properties of particulate materials, J. Microw. Power 18 (1983) 143–152.

[39] D. Gershon, J.P. Calame, A. Birnboim, Complex permittivity measurements and mixing laws of alumina composites, J. Appl. Phys. 89 (2001) 8110–8116.

[40] C. Brosseau, P. Queffelec, P. Talbot, Microwave characterization of filled polymers, J. Appl. Phys. 89 (2001) 4532–4540.

[41] K.K. Karkkainen, A.H. Sihvola, K.I. Nikoskinen, Effective permittivity of mixtures: numerical validation by the FDTD method, IEEE Trans. Geosci. Remote Sens. 38 (2000) 1303–1308.

[42] L. Landau, E. Lifshitz, Electrodynamics of Continuous Media, 2nd edition, Pergamon Press, New York, 1984.

[43] H. Looyenga, Dielectric constants of heterogeneous mixtures, Physica 31 (1965) 401–406.

[44] Z.-M. Dang, Y. Shen, C.-W. Nan, Dielectric behavior of three-phase percolative Ni–$BaTiO_3$/polyvinylidene fluoride composites, Appl. Phys. Lett. 81 (2002) 4814–4816.

[45] G. Stiubianu, C. Racles, M. Cazacu, B.C. Simionescu, Silicone-modified cellulose. Crosslinking of cellulose acetate with poly[dimethyl(methyl-H)siloxane] by Pt-catalyzed dehydrogenative coupling, J. Mater. Sci. 45 (2010) 4141–4150, doi:http://dx.doi.org/10.1007/s10853-010-4503-7.

[46] Q. Wang, M. Tahir, L. Zhang, X. Zhao, Electro-creasing instability in deformed polymers: experiment and theory, Soft Matter 7 (14) (2011) 6583–6589, doi:http://dx.doi.org/10.1039/C1SM05645J.

[47] A. Bele, M. Cazacu, G. Stiubianu, S. Vlad, M. Ignat, Polydimethylsiloxane-barium titanate composites: preparation and evaluation of the moisture, thermal, mechanical and dielectric behavior, Composites: Part B 68 (2015) 237–245.

[48] J. Crank, The Mathematics of Diffusion, 2nd ed., Oxford, Clarendon Press, 1975.

[49] C.M. Balik, On the extraction of diffusion coefficients from gravimetric data for sorption of small molecules by polymer thin films, Macromolecules 29 (1996) 3025–3029, doi:http://dx.doi.org/10.1021/ma9509467.

[50] R. Vertechy, M., Fontana, G., Stiubianu, M., Cazacu, Open-Access Dielectric Elastomer Material Database, in: Yoseph Bar-Cohen (Ed.) Proc. SPIE 9056, Electroactive Polymer Actuators and Devices (EAPAD) 2014, 90561R. http://dx.doi.org/10.1117/12.2045053.